Inactivation of CREBBP expands the germinal center B cell compartment, down-regulates MHCII expression and promotes DLBCL growth

Hashwah, Hind ; Schmid, Corina A ; Kasser, Sabrina ; Bertram, Katrin ; Stelling, Anna ; Manz, Markus G ; Müller, Anne

Abstract: The genes encoding the histone acetyl-transferases (HATs) CREB binding protein (CREBBP) and EP300 are recurrently mutated in the activated B cell-like and germinal center (GC) B cell-like subtypes of diffuse large B cell lymphoma (DLBCL). Here, we introduced a patient mutation into a human DLBCL cell line using CRISPR and deleted Crebbp and Ep300 in the GC B cell compartment of mice. CREBBP-mutant DLBCL clones exhibited reduced histone H3 acetylation, expressed significantly less MHCII, and grew faster than wild-type clones in s.c. and orthotopic xenograft models. Mice lacking Crebbp in GC B cells exhibited hyperproliferation of their GC compartment upon immunization, had reduced MHCII surface expression on GC cells, and developed accelerated MYC-driven lymphomas. Ep300 inactivation reproduced some, but not all, consequences of Crebbp inactivation. MHCII deficiency phenocopied the effects of CREBBP loss in spontaneous and serial transplantation models of MYC-driven lymphomagenesis, supporting the idea that the mutational inactivation of CREBBP promotes immune evasion. Indeed, the depletion of CD4(+) T cells greatly facilitated the engraftment of lymphoma cells in serial transplantation models. In summary, we provide evidence that both HATs are bona fide tumor suppressors that control MHCII expression and promote tumor immune control; mutational inactivation of CREBBP, but not of EP300, has additional cell-intrinsic engraftment and growth-promoting effects.

DOI: https://doi.org/10.1073/pnas.1619555114

Originally published at:
Hashwah, Hind; Schmid, Corina A; Kasser, Sabrina; Bertram, Katrin; Stelling, Anna; Manz, Markus G; Müller, Anne (2017). Inactivation of CREBBP expands the germinal center B cell compartment, down-regulates MHCII expression and promotes DLBCL growth. Proceedings of the National Academy of Sciences of the United States of America, 114(36):9701-9706.
DOI: https://doi.org/10.1073/pnas.1619555114

Inactivation of the histone acetyl-transferase CREBBP expands the germinal center B-cell compartment, down-regulates MHCII expression and promotes DLBCL initiation and growth

Hind Hashwah,[a] Corina A. Schmid,[a,*] Sabrina Kasser,[a] Katrin Bertram,[a] Anna Stelling,[a] Markus G. Manz[b] and Anne Müller[a]

[a]Institute of Molecular Cancer Research and [b]Department of Hematology, University of Zürich, Zürich, Switzerland

[*]Current address: Roche Innovation Center Zurich, Schlieren, Switzerland

For correspondence: Anne Müller, Institute of Molecular Cancer Research, Univ. of Zürich, Winterthurerstr. 190, 8057 Zürich, Switzerland; mueller@imcr.uzh.ch; phone: ++41 44 635 3474; fax: ++41 44 635 3484

Running title: Histone acetyl-transferases in DLBCL pathogenesis

Abbreviations: DLBCL, diffuse large B-cell lymphoma; HAT, histone acetyl-transferase; CREBBP, CREB binding protein, NGS, next generation sequencing; NSG, nod/scid/common gamma chain knock out

Classification: Biological Sciences: Medical Sciences

Abstract: 201 words; character count: 42836 (including spaces)

Abstract

The genes encoding the histone acetyl-transferases (HATs) CREBBP and EP300 are recurrently mutated in the activated B-cell-like and germinal center (GC) B-cell-like subtypes of diffuse large B-cell lymphoma (DLBCL). Here we introduced a patient mutation into a human DLBCL cell line using CRISPR and deleted *Crebbp* and *Ep300* in the GC B-cell compartment of mice. CREBBP-mutant DLBCL clones exhibited reduced histone H3 acetylation, expressed significantly less MHCII and grew faster than wild type clones in subcutaneous and orthotopic xenograft models. Mice lacking Crebbp in GC B-cells exhibited hyperproliferation of their GC compartment upon immunization, had reduced MHCII surface expression on GC cells, and developed accelerated MYC-driven lymphomas. Ep300 inactivation reproduced some, but not all, consequences of Crebbp inactivation. MHCII deficiency phenocopied the effects of CREBBP loss in spontaneous and serial transplantation models of MYC-driven lymphomagenesis, supporting the idea that the mutational inactivation of CREBBP promotes immune evasion. Indeed, the depletion of $CD4^+$ T-cells greatly facilitated the engraftment of lymphoma cells in serial transplantation models. In summary, we provide evidence that both HATs are *bona fide* tumor suppressors that control MHCII expression and promote tumor immune control; mutational inactivation of CREBBP, but not of EP300, has additional cell-intrinsic engraftment and growth-promoting effects.

Keywords: diffuse large B-cell lymphoma, epigenetic regulation of gene expression, histone acetylation, tumor suppressor, genome editing

Significance statement

Genes encoding chromatin-modifying enzymes such as the histone acetyl-transferases (HATs) are often mutated in diffuse large B-cell lymphoma (DLBCL), the most common lymphoma of adults. Here, we shed light on the tumor suppressive activity of HATs in human DLBCL cell lines and in mice. Cell lines harboring an experimentally introduced patient mutation in the HAT *CREBBP* lose their MHCII expression and form tumors faster in subcutaneous and orthotopic xenograft models. Mice that lack *Crebbp* specifically in the germinal center B-cell compartment also lose their MHCII expression in that compartment, and show hyper-proliferation of germinal center B-cells upon immunization, which predisposes them to MYC-driven lymphomagenesis. Our data implicate HATs as novel tumor suppressors in DLBCL.

\body

Introduction

Perturbations of the epigenome due to mutations occurring in histone-modifying enzymes are emerging as a driving force in the pathogenesis of diffuse large B-cell lymphoma (DLBCL) (1). The two main cell-of-origin subtypes of DLBCL, the activated B-cell- (ABC) and germinal center B-cell-like (GCB) subtype, are both commonly affected by mutations in epigenetic modifiers (2). The most common recurrent somatic mutations in histone-modifying enzymes are loss-of-function mutations of the histone methyltransferase (HMT) *KMT2D* (also known as *MLL2*), gain-of-function mutations of the HMT *EZH2*, and loss-of-function mutations of the histone acetyltransferases *CREBBP* and *EP300*. Together, these somatic mutations occur in approximately 50% of DLBCL patients (2), and are believed to be founder events that predispose normal B-cells to malignant transformation (1). DLBCL is characterized by extraordinary genetic diversity, both within and across tumors, which has been linked largely to the activity of activation-induced cytidine deaminase (AID), the enzyme responsible for introducing mutations in the immunoglobulin locus and thereby enabling the formation of high-affinity antibodies, and its effects on non-immunoglobulin genes (3). More recently however, epigenetic heterogeneity has emerged as an equally important hallmark of DLBCL, with strong evidence for diversity in both DNA modifications (especially cytosine methylation) and the post-translational modifications of histones. A higher degree of inter- and intratumoral heterogeneity has been associated directly with disease aggressiveness, likelihood of relapse and inferior patient survival (4-6).

The contribution of mutations in histone-modifying enzymes to DLBCL initiation and progression is subject to intense investigation. Loss-of-function mutations in *KMT2D* disrupt histone H3 lysine K4 (H3K4) mono- and dimethylation and mostly affect gene enhancer regions, promoting the proliferation of GC B-cells and preventing their terminal differentiation (7). *KMT2D* mutations occur

in 23-32% of DLBCL patients (2, 8) and are even more common in follicular lymphoma (FL); in animal models, KMT2D loss synergizes with BCL2 to accelerate lymphomagenesis (7). Lymphomas from patients with gain-of-function *EZH2* mutations show aberrant repression of GC-specific proliferation checkpoint genes and mice engineered to express mutant EZH2 exhibit a massive expansion of GC B-cells due to aberrant proliferation and differentiation blockade (9). Mutations in *CREBBP* and *EP300* affect over 30% of DLBCL as well as FL patients, and usually remove or inactivate the histone acetyl-transferase (HAT) coding domain of either gene (10); CREBBP in particular has been shown to function as part of an enhancer/super-enhancer network that regulates GC/post-GC cell fate decisions, plasma cell differentiation and antigen presentation by opposing the suppressive activities of BCL6/SMRT/HDAC3 complexes (11, 12).

Here we have investigated the mutational status of *CREBBP* and *EP300* in a panel of 11 DLBCL cell lines relative to their H3 acetylation. CRISPR technology was used to edit the *CREBBP* locus in a wild type cell line and *CREBBP*-mutant and wild type DLBCL clones were subjected to xenotransplantation studies in subcutaneous and orthotopic models. We further generated mice with a *Crebbp* deletion specifically in the germinal center B-cell compartment and assessed the contribution of Crebbp or MHCII loss, and of $CD4^+$ T-cell depletion, to lymphomagenesis in spontaneous and serial transplantation models driven by the overexpression of MYC. All available evidence from the various models implicates the HATs as important novel tumor suppressors in DLBCL pathogenesis.

Results

The *CREBBP* and *EP300* genomic loci are recurrently mutated in DLBCL cell lines, which affects histone H3 acetylation and HLA expression

To determine the mutational status of a panel of 11 DLBCL cell lines, we performed targeted re-sequencing of the 31 exons each of the *CREBBP* and *EP300* genomic loci (Fig. 1*A*). Only two of the 11 cell lines, U-2932 and OCI-Ly3, were found to be wild type for both alleles each of *CREBBP* and *EP300*, indicating that mutations targeting these loci were even more common in our panel of cell lines (>80%; Fig. 1*A*) than in previously examined DLBCL patient cohorts (2, 10). The two *CREBBP/EP300*-wild type cell lines U-2932 and OCI-Ly3 expressed clearly detectable amounts of full length CREBBP and EP300 (Fig. 1*B*). Of the remaining nine cell lines, three exhibited mono- or bi-allelic mutations or deletions of *EP300*, leading to the partial (SU-DHL-10) and complete (SU-DHL-2, RC-K8) loss, respectively, of EP300 expression (Fig. 1*B*). The acetylation of H3 on residues K18 and 27, and to some extent on K14, was reduced in the three *EP300*-mutant cell lines relative to the two wild type cell lines (Fig. 1*B*), whereas the acetylation level of K9 did not mirror the other three residues (Fig. S1*A*). The remaining six DLBCL cell lines exhibited evidence of mono-allelic (5/6) or bi-allelic (1/6) mutational inactivation of *CREBBP* by either truncating mutations leading to immature stop codons, or amino acid substitutions or chromosomal translocations that detectably affect CREBBP expression levels (Fig. 1*A,B*). Reduced or prematurely truncated CREBBP expression coincided with strongly reduced H3K14, 18 and 27 acetylation in all *CREBBP*-mutant cell lines (Fig. 1*B*), with the notable exception of SU-DHL-6, which maintains high level CREBBP expression due to a trisomy of chromosome 16. Interestingly, mutations in *CREBBP* and *EP300* were mutually exclusive in our cell line panel as had been shown previously in primary DLBCL samples (2, 10), and the loss of just one of the total of four *CREBBP*/*EP300* alleles was sufficient to produce a clear phenotype in terms of H3K14, 18 and 27 acetylation (Fig. 1*A,B*). In contrast, the acetylation of P53, which has previously been attributed to HATs and their putative activity on non-histone targets (10), was not affected by

single copy losses of *CREBBP* or *EP300* (Fig. S1*B*). ABC- and GCB-DLBCL-derived cell lines were equally affected by *CREBBP*/*EP300* mutational inactivation.

To assess in a more controlled setting whether CREBBP and EP300 expression affects H3 acetylation and histone modification-dependent target gene expression, we used RNA interference to silence both HATs in the wild type cell line U-2932. The specific depletion of CREBBP or EP300, or of both HATs combined, reduced H3K14, K18 and K27 acetylation (Fig. 1*C*, Fig. S1*C-F*). A genomic locus that is believed to be regulated by histone acetylation in B-cells, especially on residues modified by CREBBP/EP300, is the *HLA* locus. Chromatin immunoprecipitation using H3K18-acetyl-specific and H3K27-acetyl-specific antibodies followed by qPCR confirmed that the *CREBBP*/*EP300*-wild type cell line U-2932 indeed exhibits strong acetylation of K18 and K27 at regulatory elements upstream of the *HLA-DRA* transcription start site, but not at downstream regions of the gene or the MyoD control gene (Fig. 1*D*). The loss of CREBBP and EP300 expression significantly reduced HLA transcript levels, but did not affect an irrelevant control gene (Fig. 1*E*). The combined results indicate that the *CREBBP* and *EP300* genomic loci are recurrently mutated in both ABC- and GCB-DLBCL cell lines, and that their gene products contribute to histone H3 acetylation and promote active transcription in DLBCL cells at a locus known to be specifically regulated by this epigenetic mechanism.

Genome editing of *CREBBP* mimicking a patient mutation reduces histone acetylation and HLA expression, but does not affect *in vitro* growth kinetics

We next devised a strategy that allowed us to mutate one allele of the *CREBBP* locus in the wild type U-2932 cell line and to thereby mimic a previously identified patient mutation, at position A4171T, leading to a premature truncation of CREBBP at amino acid K1323X and the loss of a functional HAT domain. We aimed to mutate only one allele because most patient mutations in *CREBBP* and *EP300* are mono-allelic. Genome editing was accomplished by CRISPR technology using guide RNAs that were designed to promote the excision of exon 23, one of 12 exons encoding the HAT domain of

CREBBP (Fig. S2*A*). In five of >100 examined clones the excision event had resulted in a frame shift leading to a premature (mono-allelic) truncation of CREBBP. The resulting protein lacks the C-terminus and more than half of the HAT domain (Fig. 2*A*, Fig. S2*B*). Whereas control, unedited clones expressed copious amounts of full length CREBBP, the mutant clones exhibited a clear reduction of full length CREBBP and instead featured an extra band representing the truncated protein (Fig. 2*A*). The expression of EP300 was not affected by genomic editing of the *CREBBP* locus, with the exception of one clone (Fig. 2*A*). As expected, H3 acetylation was reduced in the clones expressing full length CREBBP from only one allele relative to the wild type clones (Fig. 2*A*). Transcriptional profiling of five mutant and five wild type clones by RNA sequencing revealed over 100 strongly differentially regulated genes due to partial loss of CREBBP activity (Fig. 2*B*, Dataset S1, GEO accession number GSE89879). The dominant biological process as determined by gene ontology analysis was “antigen processing and presentation”, as numerous MHCII genes, as well as the master regulator of MHCII expression, *CIITA*, were among the most differentially regulated genes (Fig. 2*B*). Loss of MHCII expression due to CREBBP loss was confirmed by qRT-PCR for HLA-DRA and HLA-DRB1 transcripts (Fig. 2*C*), confirming the results obtained by siRNA-mediated knock-down of CREBBP and EP300. Other interesting CREBBP target genes (downregulated in mutant clones) include *CREBBP* itself and the surface receptors *CD19, CD74, S1PR1, IFNAR2* and *CD52*. Surprisingly, almost half of dysregulated genes were up-regulated in the mutant clones despite the fact that CREBBP adds active (rather than repressive) histone marks (Fig. 2*B*, Dataset S1). We next examined the growth properties of the ten clones under various culture conditions *in vitro*; all clones grew equally fast in standard cell culture media, irrespective of their *CREBBP* status (Figure S2*C,D*), and even under exposure to the histone deacetylase (HDAC) inhibitors PBA or VPA (Fig. S2*E,F*). Similarly, we could not detect differential susceptibility to HDAC inhibitors of our *CREBBP/EP300* wild type and mutant cell lines (Fig. S2*G,H*). The combined results indicate that HAT inactivation has profound effects on global histone H3 acetylation and affects the expression of numerous genes, most notably MHCII genes, but does not confer obvious growth advantages in *in vitro* culture systems.

Monoallelic *CREBBP* inactivation promotes subcutaneous and orthotopic growth of xenografted DLBCL cell lines in immunocompromised mice

We next subcutaneously transplanted a subset of *CREBBP*-mutant and wild type clones onto the flanks of NSG mice, and determined the tumor growth over time and at the study end point. *CREBBP*-mutant clones grew faster, and had reached a larger tumor weight and volume at the study endpoint than wild type clones (Fig. 3*A*, Fig. S3*A*). The same effect was observed in a mouse strain expressing various human cytokines that have been knocked into the respective murine loci (termed MISTRG mice due to knock-in of *M-CSF, IL-3, Sirp1a, thrombopoietin, GM-CSF* in the $Rag2^{-/-}IL2Rg^{-/-}$ background (13)) (Fig. 3*B*, Fig. S3*B*). We next assessed whether U2932 clones would engraft in lymphoid organs of mice upon intravenous delivery; in NSG mice this was only the case after subcutaneous passaging, as had been described previously (14). Interestingly, subcutaneously passaged $CREBBP^{+/-}$ clones engrafted more readily than their $CREBBP^{+/+}$ counterparts in recipient bones (Fig. S3*C*), indicating that CREBBP loss may confer a growth advantage in this orthotopic but passage-dependent model. Most notably, however, we observed that both *CREBBP*-wild type and –mutant clones engrafted in the bone marrow of MISTRG mice even without prior passaging (Fig. 3*C*), with involvement of the kidneys and ovaries observed in some, but not all mice (Fig. S3*D*); involvement of other lymphoid organs such as the spleen was not observed with U2932 cells. $CREBBP^{+/-}$ clones engrafted more readily than $CREBBP^{+/+}$ clones in the bone marrow of MISTRG mice (Fig. 3*C*), suggesting that the loss of CREBBP confers a growth advantage in this novel orthotopic model. Interestingly, *CREBBP*–mutant clones exhibited lower HLA-DR expression even after extended growth *in vivo* (Fig. 3*D*). hCD20 was stained for comparison, and did not differ among mutant and wild type clones (Fig. 3*D*). The combined results suggest that *CREBBP* inactivation confers a growth advantage *in vivo* despite comparable *in vitro* growth rates, and introduce a novel model of DLBCL xenotransplantation that supports orthotopic growth without prior conditioning of human lymphoma cells.

Germinal center B-cell hyperproliferation and loss of MHCII expression upon deletion of *Crebbp*

We next sought to establish a mouse model that would allow the specific mono- and bi-allelic deletion of *Crebbp* and *Ep300* in the germinal center (GC) B-cell compartment. To this end, we crossed mice expressing Cre recombinase under the activation-induced cytidine deaminase promoter (*AID*-Cre) with mice harboring floxed *Crebbp* or *Ep300* alleles. The composite strains were immunized intraperitoneally with sheep red blood cells (SRBCs) to induce *AID*-Cre activity and GC formation. The expected excision of floxed alleles due to *AID*-Cre activity in the GC compartment was verified by the parallel immunization of *AID*-Cre x loxP-stop-loxP-RFP reporter mice (Fig. S4*A,B*). Five consecutive rounds of SRBC immunization induced GC formation in the spleen and an increase in $CD19^{+}CD95^{+}CD38^{low}$ GC B-cells (Fig. 4*A,B*). Interestingly, the deletion of one or both alleles of *Crebbp* led to hyperproliferation of the GC compartment relative to *Crebbp*-proficient animals; this effect was observed for all GC B-cells (Fig. 4*A*,*B*), irrespective of which of three alternative gating strategies was used to identify them (Fig. S4*C*), as well as for centroblasts and centrocytes that were differentiated based on their CD86 and CXCR4 expression (Fig. 4*B*, Fig. S4*C,D*). The plasmablast and plasmacyte pools increased due to immunization but were not visibly affected by loss of *Crebbp* (Fig. S4*E,F*). Strikingly, quite the opposite effects were observed upon deletion of one or both alleles of *Ep300*: *Ep300*-deficient mice generated lower numbers of GC B-cells, centroblasts and centrocytes upon immunization (Fig. 4*A,B,* Fig. S4*D*). To obtain additional complementary information on the GC compartment of the same mice, we stained spleen sections cut at various depths for Ki67 and quantified GC numbers and size; this approach revealed that the size of individual GCs, but not their multiplicity, accounts for the increase in GC B-cells in *Crebbp*-mutant mice, and the decrease in *Ep300*-mutant mice (Fig. 4*C*, Fig. S4*G*).

GC B-cells lacking one or both alleles of either *Ep300* or *Crebbp* further exhibited reduced MHCII expression relative to *Crebbp/Ep300*-proficient GC B-cells; this was true for all GC B-cells, and

especially for centroblasts (Fig. 4*D*,*E,* Fig. S4*H*). The loss of *Ep300* mirrored the effects of *Crebbp* loss on MHCII expression (Fig. 4*D*,*E,* Fig. S4*H*). Finally, to examine whether the loss of *Crebbp* would promote MYC-driven lymphomagenesis, we crossed AID-Cre x Crebbp$^{fl/wt}$ mice with a mouse strain that expresses MYC under the control of the immunoglobulin heavy chain enhancer (Emu-MYC) (15). Interestingly, the loss of one *Crebbp* allele was sufficient to significantly accelerate the formation of MYC-driven nodal B-cell lymphomas but was not sufficient to induce lymphomas in the absence of this second hit (Fig. 4*F*); furthermore, we found that upon intravenous transplantation of equal numbers of tumor cells from *Crebbp*-proficient or -deficient lymphoma-bearing donors, the latter cells engrafted more readily in the lymph nodes and spleens of wild type recipient mice, and retained their low MHCII expression relative to *Crebbp*-proficient cells (Fig. 4*G*, Fig. S4*I*). We conclude from the combined results that HATs control MHCII expression in both human and murine B-cells and that the loss of Crebbp, but not of Ep300, additionally contributes to the immunization-induced expansion of the GC compartment; both phenomena appear to predispose to malignant transformation.

The loss of MHCII expression, or CD4$^+$ T-cell depletion, promotes MYC-driven lymphomagenesis

To address whether the loss of MHCII expression that results from HAT inactivation promotes lymphomagenesis, we crossed mice lacking MHCII with Emu-MYC mice. MHCII$^{-/-}$ mice developed MYC-driven tumors earlier than their MHCII$^{+/+}$ littermates; however, the fraction of mice that did not develop lymphomas at all in the time frame of observation (80 days) was comparable in the two groups (Fig. 5*A*). MHCII$^{-/-}$ mice lack MHCII-restricted CD4$^+$ T-cells in all lymphoid tissues (Fig. S5*A*), which might explain their enhanced predisposition to MYC-driven lymphomagenesis. To dissect whether the loss of MHCII affects lymphomagenesis in immunocompetent mice with normal CD4$^+$ T-cell frequencies, we transplanted 100.000 MHCII$^{-/-}$ or MHCII$^{+/+}$ MYC-expressing tumor cells pooled from the axillary and inguinal lymph nodes of two donors per genotype into wild type C57BL6 recipients and recorded the tumor incidence. Whereas only 2 out of 16 recipients of MHCII$^{+/+}$ cells

developed lymphomas with this low dose of cells, 10 of 17 recipients of MHCII$^{-/-}$ cells did (Fig. 5*B*). The differential engraftment of MHCII-proficient and –deficient cells was reflected in on average significantly higher spleen and lymph node weights of recipients of MHCII$^{-/-}$ cells, and more efficient engraftment of tumor cells in bone marrow (Fig 5*C*). Finally, to confirm that MHCII-restricted T-cells indeed control lymphomagenesis in the serial transplantation model, we depleted CD4^{+} T-cells starting at either one day before injection of a saturating dose of 1 Mio tumor cells, or once palpable tumors had formed in the inguinal and axillary lymph nodes on day 11 post transplantation. The depletion of CD4^{+} T-cells was efficient in all examined organs (Fig. S5*B*) and strongly enhanced lymphoma cell engraftment and growth in lymph nodes, spleen and bone marrow, especially if T-cells were depleted from the start of the experiment (Fig. 5*D*). The combined results are consistent with the notion that the loss of MHCII expression confers a tumor cell survival benefit, especially during lymphoma initiation, indicating that immune surveillance driven by CD4^{+} T-cells limits lymphomagenesis in immunocompetent animals.

Discussion

In this study, we have combined targeted re-sequencing of the genes encoding the HATs CREBBP and EP300 with experimental approaches using cell cultures and mouse models to shed light on the potential tumor suppressive activity of HATs in DLBCL. As expected from previous studies using patient cohorts (2, 8, 10), our panel of 11 DLBCL cell lines confirmed that inactivating mutations in *CREBBP* and *EP300* are common, mono-allelic and mutually exclusive and typically compromise the enzymatic activity of both enzymes, leading to strongly reduced levels of histone H3 acetylation of the lysine residues K14, K18 and K27. The siRNA-mediated knockdown of CREBBP, alone and especially in combination with EP300, strongly reduced global H3 acetylation at the same three residues, but did not affect the acetylation of non-histone proteins.

To model HAT function in DLBCL cell lines in a manner that would recapitulate the dosage effect of mono-allelic mutational *CREBBP* inactivation and a possible dominant negative effect of truncated protein resulting from the introduction of premature stop codons, we introduced a typical patient mutation mono-allelically into a *CREBBP/EP300*-wild type cell line. The expression of truncated CREBBP resulted in reduced global H3K18 acetylation and large changes in gene expression. The dominant category of dysregulated genes contained the various alleles of *MHCII* genes involved in antigen presentation, as well as their master regulator, the transcription factor CIITA, which could be confirmed not only by targeted qRT-PCR in the human DLBCL cell line clones, but also in murine germinal center (GC) B-cells upon Cre-mediated excision of *Crebbp* or *Ep300*. The dependence of MHCII expression on active histone marks added by HATs thus appears to be a universal feature of murine and human B-cells, which could further be confirmed experimentally by chromatin immunoprecipitation of the *HLA-DRA* locus with acetyl-H3-specific antibodies. The transcriptional signature we identified here to be linked to CREBBP-mediated histone modification is consistent with previous reports showing that CREBBP regulates super-enhancer networks with central roles in GC/post-GC cell fate decisions, including genes involved in signal transduction by the B-cell receptor

and CD40 receptor, transcriptional control of GC and plasma cell development, and antigen presentation (11, 12).

The reduced expression of MHCII is an obvious, but not the only consequence of HAT inactivation in *CREBBP*-mutant DLBCL cell lines. Mutant clones grow faster when subcutaneously transplanted into NSG mice and *CREBBP*-mutant tumors are larger and heavier at the study endpoint than wild type tumors. The same was true in $Rag2^{-/-}\gamma c^{-/-}$ mice that express several human cytokines, allowing for efficient engraftment of various human immune cell compartments (13). The differential growth in both xenograft models is unlikely to be due to immune evasion caused by MHCII downregulation, a mechanism that has been proposed to explain the lack of T-cell activation and proliferation in *CREBBP*-mutant FL (16). In FL, *CREBBP* mutations are known to occur within the earliest inferable progenitor, result in decreased MHCII expression on tumor B-cells, and correlate with decreased frequencies of tumor-infiltrating $CD4^+$ helper T-cells (16). As anti-tumor immunity driven by $CD4^+$ T-cells can be ruled out in the two immunocompromised xenograft models used here, *CREEBP*-mutant tumors must benefit from additional cell-intrinsic growth advantages conferred by loss of HAT activity in this setting. The same was observed in genetically manipulated mice, where the loss of one or both alleles of *Crebbp* led to hyperproliferation of the GC B-cell compartment upon immunization. The dysregulated expansion of the GC compartment likely provides a setting in which additional mutations can accumulate and early clonal lesions can arise, especially given the genomic instability that is an inherent feature of GC B-cells; indeed, *Crebbp* loss accelerated MYC-driven lymphomagenesis in both spontaneous and serial transplantation models. We hypothesize that *CREBBP* mutations confer two distinct benefits during DLBCL pathogenesis, one promoting unrestricted growth during the GC reaction, and the other promoting immune evasion. Our results showing enhanced engraftment of MHCII-negative, MYC-expressing lymphoma cells into immunocompetent mice provide experimental evidence for the concept that the loss of MHCII expression indeed promotes immune evasion in this setting. This result was phenocopied by $CD4^+$ T-cell depletion, indicating that MHCII-restricted T-cells control early events of lymphomagenesis in

immunocompetent hosts, either through direct cytotoxic effects on tumor B-cells or by creating a cytokine milieu that is not conducive to tumor initiation and/or progression. Interestingly, only one of the two biological functions of CREBBP appears to be shared by EP300. *Ep300* inactivation in the mouse GC compartment downregulates MHCII expression to an extent that is comparable to *Crebbp* inactivation; in contrast, the hyperproliferation of the GC compartment upon immunization was not seen in *Ep300* mutant mice, which rather exhibited a contraction of their GC B-cells. Thus, EP300 and CREBBP have both shared and distinct activities, which in turn is reflected by the much more common mutational inactivation of *CREBBP* than of *EP300* in DLBCL patients (2, 8, 10).

In addition to their role as *bona fide* tumor suppressors in DLBCL and mechanistic contribution to the control of the GC reaction and antigen presentation, wild type HAT activity also confers clear and previously unknown benefits in terms of patient survival (17). Furthermore, HAT mutational inactivation likely predicts treatment responses to novel targeted therapies with epigenetically acting drugs, such as the HDAC3 inhibitors (11, 18). In summary, our results provide evidence for two complementary tumor suppressive mechanisms in GC B-cells that depend on HAT enzymes, of which one controls proliferation in a cell-autonomous manner, and the other sensitizes malignant B-cells to $CD4^+$ T-cell-mediated tumor control.

Materials and Methods

DLBCL cell lines and targeted re-sequencing of CREBBP and EP300. The panel of DLBCL cell lines used here included five of GCB DLBCL subtype (SU-DHL-4, SU-DHL-6, SU-DHL-10, SU-DHL-16, and RC-K8) and six of ABC DLBCL subtype (U-2932, OCI-Ly3, OCI-Ly10, SU-DHL2, SU-DHL5, and RIVA). Culture conditions, transfections, CRISPR manipulations, RNA sequencing, ChIP-PCR and Western blotting techniques are all described in the supplemental methods.

Animal experimentation. The mouse strains B6.Cg-*Crebbp*^{tm1Jvd}/J, B6.129P2-*Ep300*^{tm2Pkb}/J, B6.Cg-Tg(IghMyc)22Bri/J and B6;129P2-*Aicd*^{tm1CreMnz}/J were obtained from the Jackson Laboratories. MHCII$^{-/-}$, NOD/SCID/IL2Rγ$^{-/-}$ (NSG) and M-CSF^{h};IL-3/GM-CSF^{h};hSIRPA^{tg};TPO^{h};Rag2^{-};γc^{-} (MISTRG)(13) mice were obtained from a local repository. *Ep300*$^{fl/fl}$ and *Crebbp*$^{fl/fl}$ mice were crossed to *AID*^{cre} animals and MYC-transgenic mice were crossed with MHCII$^{-/-}$ mice and *AID*^{cre} x *Crebbp*$^{fl/fl}$ mice to obtain composite strains. 6-8 week old mice were immunized 3-6 times every second week with 200µl of 10% sheep red blood cells (Innovative Research, Michigan, USA) and sacrificed 10 days after the last immunization. All flow cytometry procedures are described in the supplemental methods. For xenotransplantation studies, *CREBBP*$^{+/-}$ and *CREBBP*$^{+/+}$ U2932 clones (10x10^{6} cells in 150µl PBS) were injected subcutaneously into both flanks of 6-8 week old NSG or MISTRG mice, or intravenously into MISTRG mice in the orthotopic model. Once palpable tumors had formed in the subcutaneous model (~40 mm^{3}), the volume of the tumors was measured by calipers and calculated using the formula (a2xb)/2, where a is the shorter and b the longer tumor dimension. For serial transplantation studies, 100.000 to 1 Mio tumor cells pooled from the axillary and inguinal lymph nodes, or from spleens of mice were cryopreserved in FCS + 10% DMSO, and were subsequently injected intravenously in a volume of 100 µl. All animal studies were reviewed and approved by the Zürich Cantonal Veterinary Office (licenses 227/2015, 235/2015).

Acknowledgments

We thank Alexandar Tzankov and Darius Juskevicius for helpful discussions and comments on the manuscript. This study was funded by grants from the Zurich Cantonal and Swiss Cancer Leagues to A.M. Additional support was provided by the Clinical Research Priority Program “Human Hemato-lymphatic Diseases” of the University of Zurich.

Conflict of interest

The authors declare that no conflict of interest exists.

References

1. Jiang Y, Dominguez PM, & Melnick AM (2016) The many layers of epigenetic dysfunction in B-cell lymphomas. *Curr Opin Hematol* 23(4):377-384.
2. Pasqualucci L*, et al.* (2011) Analysis of the coding genome of diffuse large B-cell lymphoma. *Nat Genet* 43(9):830-837.
3. Chandra V, Bortnick A, & Murre C (2015) AID targeting: old mysteries and new challenges. *Trends Immunol* 36(9):527-535.
4. Chambwe N*, et al.* (2014) Variability in DNA methylation defines novel epigenetic subgroups of DLBCL associated with different clinical outcomes. *Blood* 123(11):1699-1708.
5. De S*, et al.* (2013) Aberration in DNA methylation in B-cell lymphomas has a complex origin and increases with disease severity. *PLoS Genet* 9(1):e1003137.
6. Pan H*, et al.* (2015) Epigenomic evolution in diffuse large B-cell lymphomas. *Nat Commun* 6:6921.
7. Zhang J*, et al.* (2015) Disruption of KMT2D perturbs germinal center B cell development and promotes lymphomagenesis. *Nat Med* 21(10):1190-1198.
8. Lohr JG*, et al.* (2012) Discovery and prioritization of somatic mutations in diffuse large B-cell lymphoma (DLBCL) by whole-exome sequencing. *Proc Natl Acad Sci U S A* 109(10):3879-3884.
9. Beguelin W*, et al.* (2013) EZH2 is required for germinal center formation and somatic EZH2 mutations promote lymphoid transformation. *Cancer Cell* 23(5):677-692.
10. Pasqualucci L*, et al.* (2011) Inactivating mutations of acetyltransferase genes in B-cell lymphoma. *Nature* 471(7337):189-195.
11. Jiang Y*, et al.* (2016) CREBBP Inactivation Promotes the Development of HDAC3 Dependent Lymphomas. *Cancer Discov* 7(1):38-53.
12. Zhang J*, et al.* (2017) The Crebbp Acetyltransferase is a Haploinsufficient Tumor Suppressor in B Cell Lymphoma. *Cancer Discov* 7(3):322-337.
13. Rongvaux A*, et al.* (2014) Development and function of human innate immune cells in a humanized mouse model. *Nat Biotechnol* 32(4):364-372.
14. Bosch R*, et al.* (2012) Subcutaneous passage increases cell aggressiveness in a xenograft model of diffuse large B cell lymphoma. *Clin Exp Metastasis* 29(4):339-347.
15. Adams JM*, et al.* (1985) The c-myc oncogene driven by immunoglobulin enhancers induces lymphoid malignancy in transgenic mice. *Nature* 318(6046):533-538.
16. Green MR*, et al.* (2015) Mutations in early follicular lymphoma progenitors are associated with suppressed antigen presentation. *Proc Natl Acad Sci U S A* 112(10):E1116-1125.
17. Juskevicius D*, et al.* (2017) Mutations of CREBBP and SOCS1 are independent prognostic factors in diffuse large B cell lymphoma: mutational analysis of the SAKK 38/07 prospective clinical trial cohort. *J Hematol Oncol* 10(1):70.
18. Andersen CL, Asmar F, Klausen T, Hasselbalch H, & Gronbaek K (2012) Somatic mutations of the CREBBP and EP300 genes affect response to histone deacetylase inhibition in malignant DLBCL clones. *Leuk Res Rep* 2(1):1-3.

Figure legends

Fig. 1. The mutational inactivation or deletion of *CREBBP* and *EP300* affects histone H3 acetylation and HLA expression in DLBCL cell lines. (*A*) Targeted re-sequencing of *CREBBP* and *EP300* (all 31 exons) in the panel of 11 indicated DLBCL cell lines. Chromosomal deletions and translocations are listed as reported in the literature. (*B*) Protein lysates from the DLBCL cell lines shown in A were subjected to immunoblot analysis using antibodies specific for CREBBP, EP300, α-tubulin, H3K14ac, H3K18ac, H3K27ac, and total H3. Blots shown are representative of two independent experiments. Color code in A and B: blue, wild type; black, mutant *CREBBP*; red: mutant *EP300*. Asterisks indicate truncated CREBBP protein. (*C*) U-2932 cells were treated with control siRNA or siRNAs specific for *CREBBP*, *EP300*, or both (pool); protein lysates were harvested after 72h and 96h and subjected to immunoblot analysis using the indicated antibodies. A representative experiment is shown along with the densitometric quantification of four independent experiments. (*D*) Profile of histone acetylation at the *HLA-DRA* locus. ChIP of U-2932 cells was performed with H3K18ac, H3K27ac and control IgG antibody and was followed by PCRs of the 8 regions indicated on the X-axis. (*E*) Relative expression of *HLA-DRA* and *HLA-DRB1* and of *WEE1* as control, normalized to RPLP32, as assessed by qRT-PCR of U-2932 cells treated with siRNAs for 48h as described in C. Data in C and E represent means + SD of 4 biological replicates. *p<0.05; **p<0.01; ***p<0.001; ****p<0.0001.

Fig. 2. Genome editing of *CREBBP* in U-2932 cells reduces HLA expression. (*A*) Protein lysates from four $CREBBP^{+/+}$ and five $CREBBP^{+/-}$ clones were subjected to immunoblot analysis with antibodies specific for CREBBP, EP300, α-tubulin, and H3K18ac. (*B*) Transcriptional profiling of five $CREBBP^{+/+}$ and five $CREBBP^{+/-}$ clones was performed by RNA sequencing. The top 100 most strongly differentially regulated genes (log2 ratio ≥ 0.4 and ≤ -0.4) are displayed in a heat map. Genes of the *HLA* family, as well as *CREBBP* and *CIITA* are annotated. (*C*) Relative expression of *HLA-DRA* and *HLA-DRB1*

compared to RPLP0 as assessed by qRT-PCR of the clones shown in B, plus several additional wild type clones. **p<0.01.

Fig. 3. Growth of xenografted U-2932 *CREBBP*$^{+/+}$ and *CREBBP*$^{+/-}$ clones in NSG and MISTRG mice. (*A,B*) Ten million cells of two *CREBBP*$^{+/+}$ and two *CREBBP*$^{+/-}$ clones were subcutaneously transplanted onto the flanks of NSG (*A*) or MISTRG (*B*) mice. Tumor volumes were measured with calipers every other day from day 10 until day 29 post transplantation and at the study end point. The tumor weight was determined at the study endpoint. Each symbol represents one tumor. Results from two pooled experiments are shown for each mouse strain. (*C,D*) Ten million cells of three *CREBBP*$^{+/+}$ and three *CREBBP*$^{+/-}$ clones were intravenously transplanted into MISTRG mice; mice were sacrificed at four weeks post transplantation and assessed with respect to their human tumor burden in the bone marrow (C), as well as the expression of hCD20 and HLA-DR on bone-marrow-infiltrating tumor B-cells (D). Pooled data from two studies are shown in C, and data from one of the two studies is shown in D. p-values were calculated using the Mann-Whitney test. *p<0.05; **p<0.01; ***p<0.001.

Fig. 4. **Deletion of *Crebbp* within the GC compartment promotes GC expansion, reduces MHCII expression and accelerates MYC-driven lymphomagenesis.** (*A*,*B*) Littermates with either no (wt), one (fl/wt) or two (fl/fl) floxed alleles of *Crebbp* or *Ep300,* which additionally express Cre under the control of the AID promoter, were immunized 4 times at biweekly intervals with sheep red blood cells and sacrificed 10 days after the last injection. Representative flow cytometry plots of splenic GC B-cells are shown in A, and the frequencies of CD95^{+}CD38^{low} GC B-cells, as well as of Cxcr4^{+} centroblasts (CB) are shown in % of all CD19^{+} live cells in B. Non-immunized mice are included for comparison. Pooled data from three to five independent cohorts are shown. (*C*) The GC number and GC area per spleen area (arbitrary units) of the mice shown in B, as quantified based on Ki67 staining of three spleen sections per mouse. (*D,E*) Median fluorescence intensity (MFI) of MHCII surface

expression on GC B-cells and centroblasts of the mice shown in B and C; representative histograms are shown in D. (*F*) Mice of the three indicated genotypes were immunized at regular 14 day intervals and monitored for clinical symptoms and enlarged lymph nodes indicating lymphoma development. Moribund mice were sacrificed and their survival time since the first immunization was plotted. (*G*) Four and three wild type C57BL/6 mice were i.v. injected with 0.5 Mio *Crebbp*$^{fl/wt}$ or *Crebbp*$^{wt/wt}$ MYC-expressing lymphoma cells, respectively, that were harvested from the pooled inguinal and axillary lymph nodes of lymphoma-bearing donors. Mice were assessed with respect to their lymph node weights (inguinal and axillary LNs are plotted separately for each recipient and share the same color code) and lymph node B-cell MHCII expression at the study endpoint (28 days post transplantation), relative to two non-transplanted controls. p-values were calculated using the Mann-Whitney test. *p<0.05; **p<0.01; ***p<0.001; ****p<0.0001.

Fig. 5. Tumor cell-intrinsic MHCII loss and CD4^{+} T-cell depletion both confer enhanced susceptibility to MYC-driven lymphomagenesis. (*A*) Mice of the indicated genotypes were immunized at regular 14 day intervals with sheep red blood cells and monitored for clinical symptoms and enlarged lymph nodes indicating lymphoma development. Moribund mice were sacrificed and their survival time since the first immunization was plotted. (*B,C*) 16 and 17 wild type C57BL/6 mice were i.v. injected with 0.1 Mio MHCII$^{+/+}$ or MHCII$^{-/-}$ MYC-expressing lymphoma cells, respectively, that were harvested from the pooled inguinal and axillary LNs of lymphoma-bearing donors. Mice were assessed with respect to lymphoma incidence (*B*) and spleen and LN weights (one data point per mouse, the mean of the four inguinal and axillary LNs is shown) and B-cell frequencies in bone marrow at the study endpoint (*C*, 28 days post transplantation), relative to two non-transplanted controls. Pooled data from two studies are shown in B and C, except for the BM data which were from one study only. (*D*) 18, 17 and 7 wild type C57BL/6 mice were i.v. injected with 1 Mio splenic MHCII$^{+/+}$ MYC-expressing lymphoma cells, respectively, and assessed with respect to spleen and LN weights (one data point per mouse, the mean of two inguinal and axillary LNs is shown) and B-cell frequencies in bone

marrow at the study endpoint (28 days post transplantation), relative to five non-transplanted controls. Mice were additionally treated weekly with CD4-specific or isotype control antibody, starting either at one day before transplantation, or once palpable tumors had formed (at 11 days p.t.). Pooled data from two studies are shown in D. p-values were calculated using the Mann-Whitney test. *$p<0.05$; **$p<0.01$; ***$p<0.001$.

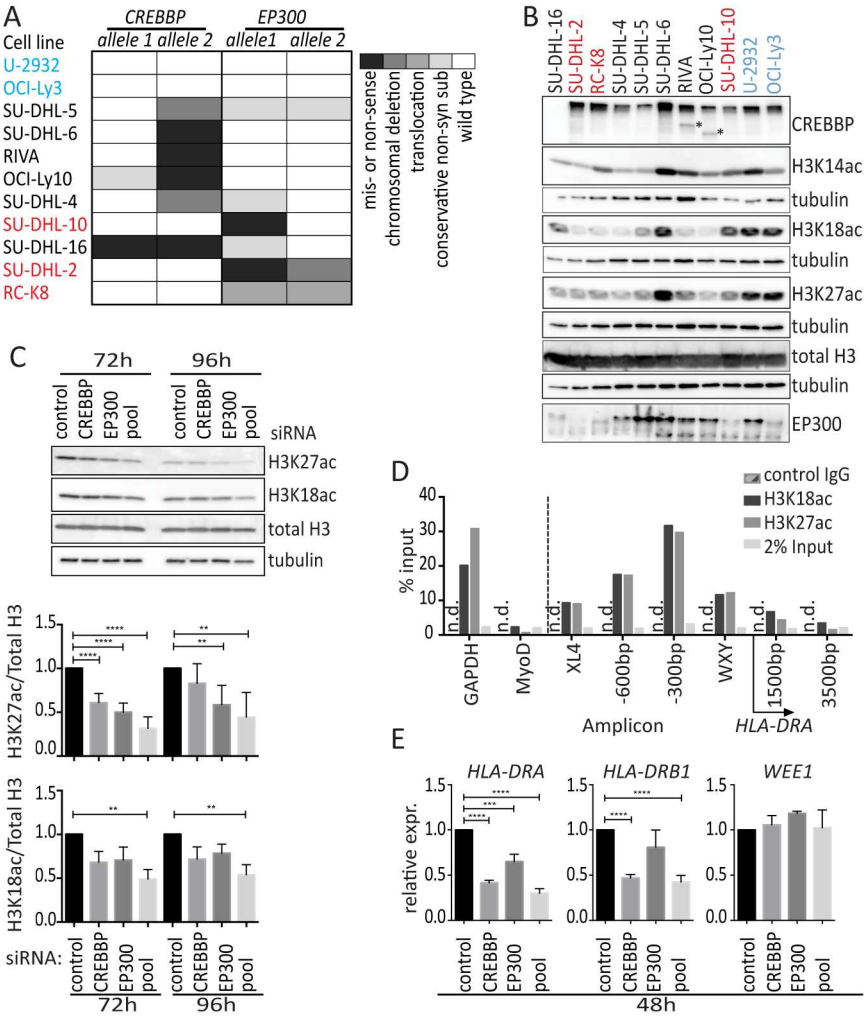
A
CREBBP
EP300
allele 1 allele 2
allele1 allele 2
Cell line
U-2932
OCI-Ly3
SU-DHL-5
SU-DHL-6
RIVA
OCI-Ly10
SU-DHL-4
SU-DHL-10
SU-DHL-16
SU-DHL-2
RC-K8
mis- or non-sense
chromosomal deletion
translocation
conservative non-syn sub
wild type
B
SU-DHL-16
SU-DHL-2
RC-K8
SU-DHL-4
SU-DHL-5
SU-DHL-6
RIVA
OCI-Ly10
SU-DHL-10
U-2932
OCI-Ly3
CREBBP
H3K14ac
tubulin
H3K18ac
tubulin
H3K27ac
tubulin
total H3
tubulin
EP300
C
72h
96h
control
CREBBP
EP300 pool
siRNA
H3K27ac
H3K18ac
total H3
tubulin
H3K27ac/Total H3
H3K18ac/Total H3
siRNA:
72h
96h
D
control IgG
H3K18ac
H3K27ac
2% Input
% input
n.d.
GAPDH
MyoD
XL4
-600bp
-300bp
WXY
1500bp
3500bp
Amplicon
HLA-DRA
E
HLA-DRA
HLA-DRB1
WEE1
relative expr.
48h

Fig. 1.

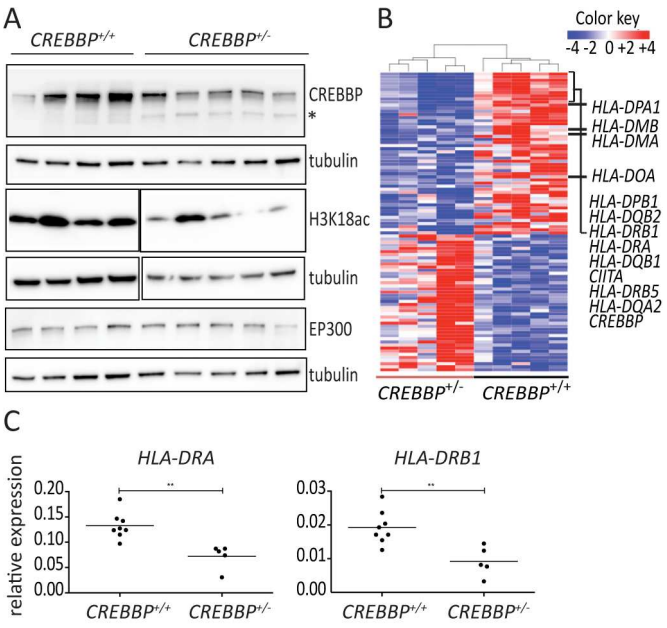
A
CREBBP+/+
CREBBP+/-
CREBBP
*
tubulin
H3K18ac
tubulin
EP300
tubulin
B
Color key
-4 -2 0 +2 +4
HLA-DPA1
HLA-DMB
HLA-DMA
HLA-DOA
HLA-DPB1
HLA-DQB2
HLA-DRB1
HLA-DRA
HLA-DQB1
CIITA
HLA-DRB5
HLA-DQA2
CREBBP
CREBBP+/-
CREBBP+/+
C
HLA-DRA
HLA-DRB1
relative expression
0.20
0.15
0.10
0.05
0.00
0.03
0.02
0.01
0.00
**
**
CREBBP+/+
CREBBP+/-
CREBBP+/+
CREBBP+/-

Fig. 2.

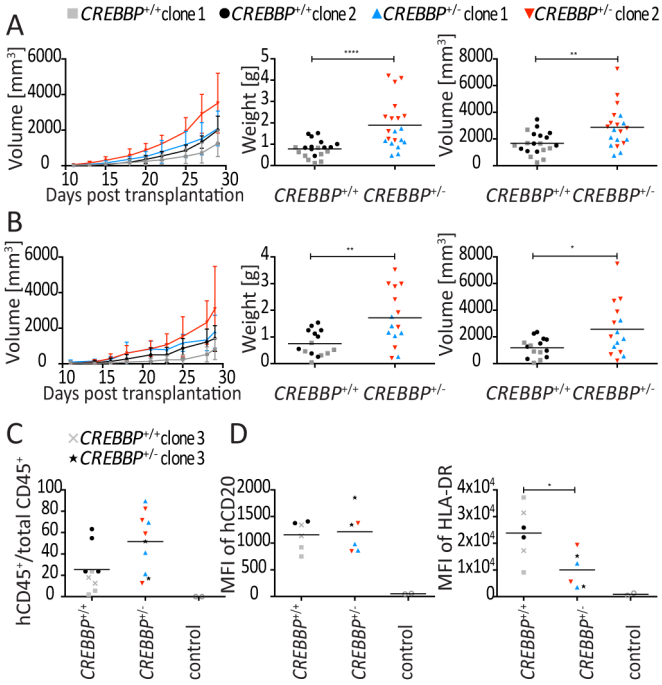
A
CREBBP+/+ clone 1
CREBBP+/+ clone 2
CREBBP+/- clone 1
CREBBP+/- clone 2
Volume [mm3]
Days post transplantation
Weight [g]
CREBBP+/+ CREBBP+/-
B
C
CREBBP+/+ clone 3
CREBBP+/- clone 3
hCD45+/total CD45+
D
MFI of hCD20
MFI of HLA-DR
CREBBP+/+
CREBBP+/-
control

Fig. 3.

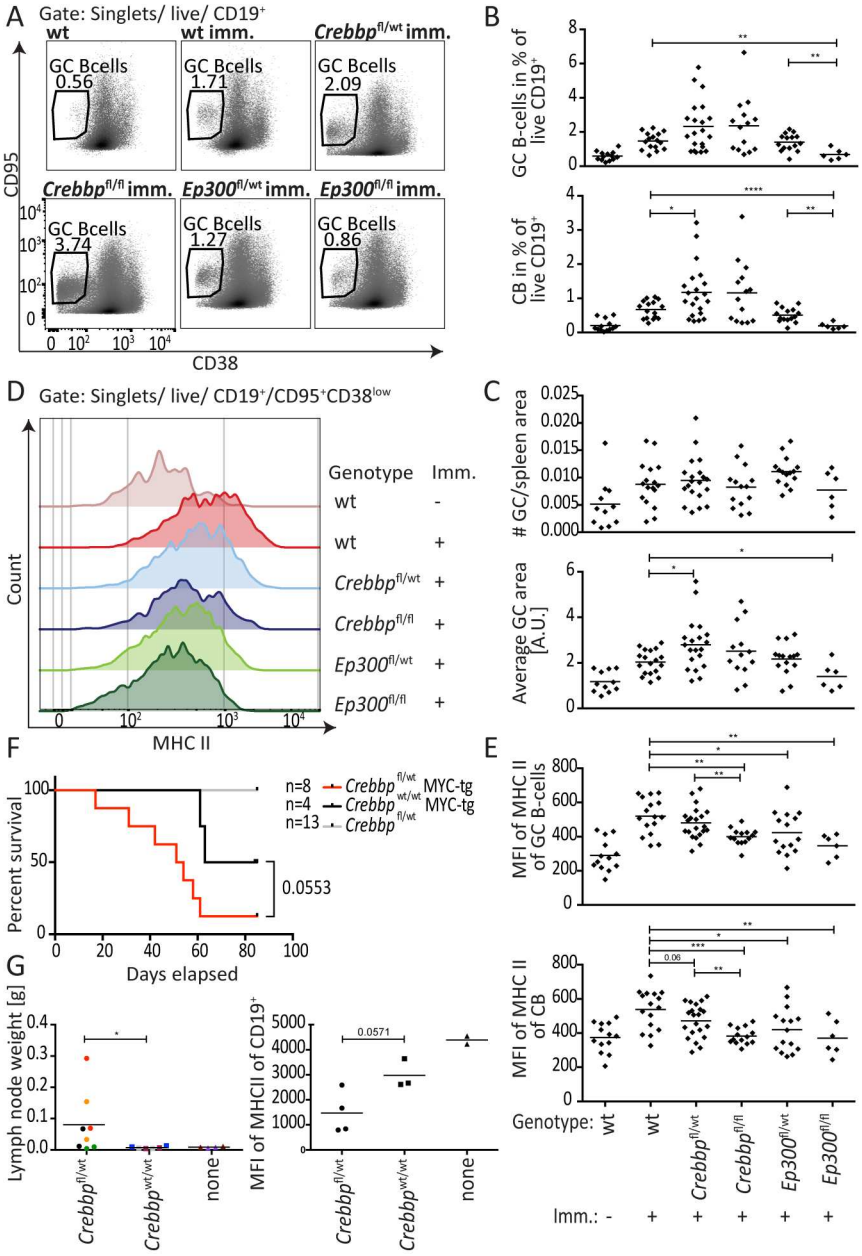
A
Gate: Singlets/ live/ CD19+
wt
wt imm.
Crebbpfl/wt imm.
Crebbpfl/fl imm.
Ep300fl/wt imm.
Ep300fl/fl imm.
GC Bcells
0.56
1.71
2.09
3.74
1.27
0.86
CD95
CD38
B
GC B-cells in % of live CD19+
CB in % of live CD19+
C
GC/spleen area
Average GC area [A.U.]
D
Gate: Singlets/ live/ CD19+/CD95+CD38low
Count
MHC II
Genotype
Imm.
wt
Crebbpfl/wt
Crebbpfl/fl
Ep300fl/wt
Ep300fl/fl
E
MFI of MHC II of GC B-cells
MFI of MHC II of CB
Genotype:
Imm.:
F
Percent survival
Days elapsed
n=8 Crebbpfl/wt MYC-tg
n=4 Crebbpwt/wt MYC-tg
n=13 Crebbpfl/wt
0.0553
G
Lymph node weight [g]
MFI of MHCII of CD19+
0.0571
none

Fig. 4.

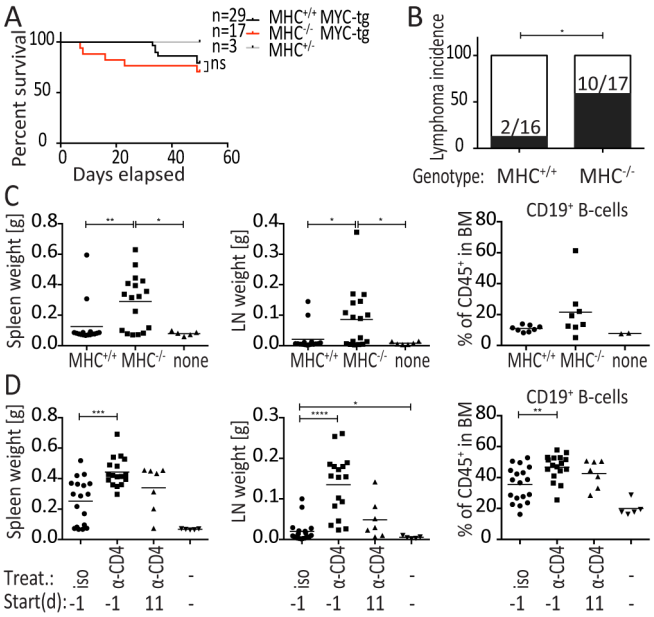
A
n=29 MHC+/+ MYC-tg
n=17 MHC-/- MYC-tg
n=3 MHC+/-
ns
Percent survival
Days elapsed
B
Lymphoma incidence
2/16
10/17
Genotype: MHC+/+ MHC-/-
C
Spleen weight [g]
LN weight [g]
CD19+ B-cells
% of CD45+ in BM
MHC+/+ MHC-/- none
D
Treat.: iso α-CD4 α-CD4 -
Start(d): -1 -1 11 -

Fig. 5.

Supporting Information

SI figure legends

Fig. S1. The histone acetyl-transferases CREBBP and EP300 regulate H3K14, but not H3K9 or p53 acetylation. (**A,B**) Protein lysates of the indicated 11 DLBCL cell lines were subjected to immunoblot analysis using antibodies for TFIIH, total p53, ac-p53, H3K9ac, and α-tubulin. Blots shown are representative of two independent experiments. (**C**) U-2932 cells were electroporated with control siRNA or siRNAs specific for CREBBP, EP300, or both (pool); protein lysates were harvested 48h post transfection and used for immunoblot analysis with antibodies specific for CREBBP, EP300, and α-tubulin. (**D**) Densitometric quantification of the knock down efficiency of CREBBP and EP300 of all four experiments shown in Figure 1C and E, as shown representatively for one experiment in C. Note that there is compensatory CREBBP expression due to EP300 depletion, but not vice versa. (**E,F**) U-2932 cells were treated with control siRNA or siRNAs specific for CREBBP, EP300, or both (pool); protein lysates were harvested after 72h and 96h and subjected to immunoblot analysis using an antibody for H3K14ac. A representative experiment of two is shown in E, along with its densitometric quantification in F. p-values were calculated using the Mann-Whitney test. *p<0.05; **p<0.01; ***p<0.001.

Fig. S2. CRISPR-mediated genome editing of *CREBBP*. (**A**) Schematic of the strategy used for excising exon 23 of *CREBBP* with CRISPR/Cas9 technology. (**B**) PCR confirmation of the deletion. (**C,D**) Viability assessment of *CREBBP* wild type and mutant clones. Five wild type and five mutant clones were seeded at a density of $0.3x10^6$/ml. Cell number/ml is shown in C; the viability as assessed by Cell Titer Blue assay is shown in D. (**E-H**) To assess the sensitivity to HDAC inhibitors, CRISPR clones (E,F) and DLBCL cell lines (G,H) were seeded at a density of $0.4x10^6$/ml and treated with either sodium 4-phenylbutuyrate (PBA) or valproic acid sodium salt (VPA) (Sigma Aldrich) at the indicated final concentrations; viability was assessed by Cell Titer Blue assay. Data in E-H are represented as means of 2 independent experiments.

Fig. S3. Growth of xenografted U-2932 *CREBBP*$^{+/+}$ and *CREBBP*$^{+/-}$ clones in NSG and MISTRG mice. (A,B) Ten million cells of two *CREBBP*$^{+/+}$ and two *CREBBP*$^{+/-}$ clones were subcutaneously transplanted onto the flanks of NSG (A) or MISTRG (B) mice. Tumor volumes were measured with calipers every other day from day 10 until day 29 post transplantation for each mouse. Each line represents one mouse. Results from two pooled experiments are shown for each mouse strain. **(C)** Six million subcutaneously passaged cells of two *CREBBP*$^{+/+}$ and two *CREBBP*$^{+/-}$ U2932 clones were intravenously transplanted into NSG mice; mice were sacrificed at four weeks post transplantation and assessed with respect to their human tumor burden in the bone marrow. **(D)** Representative images of H&E-stained sections of a tumor-bearing kidney and a healthy kidney (both from MISTRG mice) are shown. Scale bar is 1000 μm.

Fig. S4. Germinal center B-cell hyperproliferation and loss of MHCII expression upon deletion of Crebbp. (**A,B**) $AID^{cre/wt}$ and $AID^{cre/wt}$ $RFP^{fl/wt}$ mice were immunized once intraperitoneally with 200µl of 10% sheep red blood cells and sacrificed 10 days afterwards**.** The percentage of germinal center B-cells of $CD19^+$ live cells were assessed by flow cytometry. Germinal center B-cells were gated as singlets/live/$CD19^+$/$CD95^+CD38^{low}$. RFP^+ GC B cells were gated as singlets/live/$CD19^+$/ $CD95^+CD38^{low}/RFP^+$. Representative FACS plots are shown in A; the quantification of RFP^+ germinal center B-cells after immunization is shown for two independent experiments in B. Each symbol represents one mouse. Horizontal lines indicate means. Statistical analysis was done by Mann-Whitney test. (**C**) Gating strategy for germinal center (GC) B cells, centroblasts (CB), and centrocytes (CC). GC B cells can be gated using three different strategies: 1- singlets/live/$CD19^+$/$CD95^+CD38^{low}$, 2- singlets/live/$CD19^+B220^+$/$CD95^+PNA^{high}$, and 3- singlets/live/$CD19^+$/$B220^+PNA^{high}$. Centroblasts are $Cxcr4^{hi}CD86^{low}$; centrocytes are $Cxcr4^{low}CD86^{low}$. (**D**) Littermates with either no (wt), one (fl/wt) or two (fl/fl) floxed alleles of *Crebbp* or *Ep300,* which additionally express Cre under the control of the AID promoter, were immunized 4 times at biweekly intervals with sheep red blood cells and sacrificed 10 days after the last injection. Non-immunized mice are shown as controls. The quantification of centrocytes (CC) in % of live $CD19^+$ cells is shown for the animals included in main Figure 4B. (**E**) Gating strategy for plasmablasts (PB) and plasma cells (PC). Plasmablasts and plasma cells were gated as singlets/live/$CD3^-$/$CD138^+B220^+$ and singlets/live/$CD3^-$/$CD138^+B220^-$, respectively. (**F**) Quantification of the percentages of plasmablasts and plasma cells, of the mice shown in E and in Figure 4B. (**G**) Representative image of a Ki67-stained spleen. Arrows indicate germinal centers. Spleens were formalin-fixed and embedded in paraffin, and three sections per spleen approximately 100 µm apart were stained with a Ki67-specific antibody. Images were acquired on a Leica microscope. **(H)** Median fluorescence intensity (MFI) of MHCII expression of the centrocytes shown in D. In D,F and H, each symbol represents one mouse. Pooled data from three to five independent cohorts are shown. **(I)** Four and three wild type C57BL/6 mice were i.v. injected with 0.5 Mio *Crebbp*$^{fl/wt}$ or *Crebbp*$^{wt/wt}$ MYC-expressing lymphoma cells, respectively, that were harvested from the pooled inguinal and axillary lymph nodes of lymphoma-bearing donors. Mice were assessed with respect to their spleen weights and splenic B-cell MHCII expression at the study endpoint (28 days post transplantation), relative to two non-transplanted controls. p-values were calculated using the Mann-Whitney test. *p<0.05; **p<0.01; ***p<0.001.

Fig. S5. Tumor cell-intrinsic MHCII loss and $CD4^+$ T-cell depletion both confer enhanced susceptibility to MYC-driven lymphomagenesis. (A) Mice of the indicated genotypes were assessed with respect to their $CD4^+$ T-cell compartment in the blood. **(B)** 18, 17 and 7 wild type C57BL/6 mice were i.v. injected with 1 Mio splenic $MHCII^{+/+}$ MYC-expressing lymphoma cells, respectively, and additionally treated weekly with CD4-specific or isotype control antibody, starting either at one day before transplantation, or once palpable tumors had formed (at 11 days p.t.). Graphs show the $CD4^+$ T-cell depletion efficiency in the spleen, lymph nodes (LN) and bone marrow (BM); pooled data from two studies are shown. p-values were calculated using the Mann-Whitney test. *p<0.05; **p<0.01; ***p<0.001.

Dataset S1. List of 100 top significantly differentially expressed genes between *CREBBP*$^{+/+}$ and *CREBBP*$^{+/-}$ clones as identified by RNA-sequencing. The cut-off for the log2 ratio was specified as ≥ 0.4 and ≤ -0.4.

Supplemental materials and methods

DLBCL cell culture, transfection and cell viability assays

Cell lines were maintained at 37°C, 5% CO_2 in a humidified atmosphere in IMDM (RIVA, OCI-Ly3, OCI-Ly10) or RPMI (SU-DHL2 and SU-DHL5) supplemented with 10% or 20% (SU-DHL-4, SU-DHL-6, SU-DHL-10, SU-DHL-16, RC-K8, U-2932) heat-inactivated FBS and antibiotics. For the purpose of siRNA treatment, $0.5x10^6$ DLBCL cells were nucleoporated using the Amaxa Nucleofector II device such that the final concentration of siRNA was 100µM. The following siRNAs were purchased from Qiagen: Hs EP300 7 FlexiTube siRNA Cat no: SI02626267, Hs CREBBP8 FlexiTube siRNA Cat no: SI02633099 and Control AllStars Negative Control siRNA Cat no: SI03650318. Cells were harvested 48h, 72h, or 96h post transfection for protein or RNA extraction. For viability assays, cells were seeded at a density of $0.3x10^6$/ml. 50µl of cell suspension were transferred into 96-well plates containing 50µl fresh medium in triplicates. 20µl of CellTiter-Blue reagent (Promega) was added and plates were incubated for 4h at 37°C, 5% CO_2 in a humidified atmosphere. Viability was subsequently assessed by measuring fluorescence at 560Ex/590Em using a SpectraMax M5 microplate reader.

CRISPR/Cas9 manipulation of U-2932 cells

The PX458 plasmid used was obtained from Addgene (#48138: pSpCas9(BB)-2A-GFP). Guide RNAs were designed using the Zheng Lab online tool (http://crispr.mit.edu/) and cloned into PX458. Guide RNA efficiency was tested by calcium phosphate transfection of HEK 293T cells and the best gRNA combination was chosen. gRNA 1 fwd: CAC CGT GCA CTT ACC CTC ATG AC; rev: AAA CGT CAT GAG GGT AAG AAT GCA C; gRNA 2 fwd: CAC CGC AGC ATT CAG ATA GTT TGT, rev: AAA CAC AAA CTA TCT GAA TGC TGC $0.5x10^6$ U-2932 cells were nucleoporated with 3µg of the plasmid containing the desired gRNAs using the Amaxa Nucleofector II device, and 48h post transfection the cells were single cell sorted for GFP expression into pre-conditioned medium. Single cell cultures were subsequently screened by gDNA isolation (adapted from the KAPA Mouse Genotyping Kit, KAPA Biosystems), and PCR based verification of the deletion (fwd: TCA GGG TGA GTT GTT TCC CC, rev: TTA GAG AGT GCT GGC CAA CA).

RNA sequencing and data analysis

RNA from DLBCL cell lines as well as CRISPR/Cas9 edited U-2932 was isolated using the NucleoSpin RNA kit (Macherey-Nagel). RNA quality was assessed by Bioanalyzer 2100 followed by library preparation using the TruSeq RNA Sample Prep Kit v4 (Illumina). Sequencing was subsequently performed on the Illumina HiSeq 2500 instrument. RNA-seq reads were quality-checked with fastqc, which computes various quality metrics for the raw reads. RNA-seq reads were mapped to the GRCh38 reference human genome using STAR and reads were counted according to Ensembl gene annotation using the featureCounts function in the Rsubread Bioconductor package. Statistical analysis of differential expression was conducted with the DESeq2 package.

Quantitative RT-PCR

RNA was extracted using the Nucleospin RNA kit. 1µg of total RNA was reverse transcribed using SuperScriptIII reverse transcriptase (Invitrogen). For qRT-PCR, Lightcycler 480 Cyber Green Master I (Roche) was used followed by analysis on a Lightcycler 480 instrument. Samples were measured in duplicates. For all primer pairs, the efficiency was calculated by performing dilution series experiments. Target mRNA abundance was subsequently calculated relative to human RPLP0 or RPLP32. The following primers were used: RPLP0, fwd: CCA GCT CTG GAG AAA CTG CTG, rev: CAG CAG CTG GCA CCT TAT TGG; RPLP32, fwd: GAA GTT CCT GGT CCA CAA CG, rev: 5'- GCG ATC TCG GCA CAG TAA G; CREBBP, fwd: GTC CAG TTG CCA CAA GCA C, rev: CAT TCG GGA AGG AGA AAT GG; EP300, fwd: GCC AAG TAC TTC AGC TAC CCA GT, rev: GGC ATC AGT GCC TGT CGT AG; HLA-DRA, fwd: GCA CTG GGA GTT TGA TGC TC, rev: AGG GCA CAC ACC ACG TTC; HLA-DRB1, fwd: ACT ACG GGG TTG TGG AGA GC, rev: GAG CAG ACC AGG AGG TTG TG; WEE1, fwd: ATT GGC GGG CTC TGT TGA T, rev: GCC CAC GCA GAG AAA TAT CG.

Western blotting

Protein extracts were made in RIPA buffer (50mM Tris-HCl, pH 8.0, 150mM sodium chloride, 1% NP-40, 0.5% sodium deoxycholate, 0.1% SDS) supplemented with 2mM sodium orthovanadate, 15mM sodium pyrophosphate, 10mM sodium fluoride and 1X complete protease inhibitor cocktail (Roche). Protein extracts for CREBBP/EP300 were prepared in MNase buffer 1 (0.3M sucrose, 15mM Tris pH 7.5, 60mM KCl, 15mM NaCl, 5mM $MgCl_2$, 0.1mM EGTA, 05mM DTT, 0.5% NP-40, and 1% Sodium deoxycholate) + MNase buffer 2 (0.3M sucrose, 85mM Tris pH 7.5, 3mM $MgCl_2$, 2mM $CaCl_2$, and 10U S7 MNase, Roche). The reaction was stopped by addition of EDTA with a final concentration of 5mM. Protein concentrations were determined using BCA assay (Pierce) or Bradford assay (Bio-Rad) for MNase-isolated proteins, and equal amounts were separated by SDS/PAGE (4–20% Mini-PROTEAN® TGX™ Precast Protein Gels, BIO-RAD) followed by transfer onto nitrocellulose membranes. Membranes were probed with antibodies against α-tubulin (DM1A, Sigma Aldrich), p300 (N-15, Santa Cruz Biotechnology), CBP (A-22, Santa Cruz Biotechnology), TFIIH p89 (s-19, Santa Cruz Biotechnology), and p53 antibody (9282), Acetyl-p53 (Lys382), CBP (D6C5), Histone H3 XP (D1H2), Acetyl-Histone H3 Lys9 (C5B11), Acetyl-Histone H3 Lys27 XP (D5E4), Acetyl-Histone H3 Lys18 (D8Z5H), and Acetyl-Histone H3 Lys14 (D4B9) (all from Cell Signaling).

Flow cytometric analysis

Cells isolated from mouse spleens, lymph nodes, blood or bone marrow were treated with ACK red blood cell lysis buffer pH 7.2-7.4 (150mM NH_4Cl, 10mM $KHCO_3$, 0.1mM Na_2EDTA) and passed through a 40µM cell strainer to produce single-cell suspensions. Cells were subsequently stained using the following fluorescent-labeled anti-mouse antibodies: PE-Cy7 conjugated anti-CD95/FAS (Jo2, Becton Dickinson), PerCP-Cy5.5 conjugated anti-CD86 (GL-1, Biolegend), Pacific Blue™ conjugated anti-I-A/I-E (M5/114.15.2, Biolegend), Purified Rat Anti-Mouse CD16/CD32 (93, Biolegend), Brilliant Violet™ 650 anti-CD45 (30-F11, Biolegend), Brilliant Violet™ 605 anti-CD4 (RM4-5, Biolegend), PE-Cy7 anti-TCR-beta chain (H57-597, Biolegend), APC anti-CD8a (53-6.7, Biolegend), FITC anti-CD19 (1D3, Biolegend), Alexa Fluor® 700 anti-I-A/I-E (M5/114.15.2, Biolegend), FITC anti-CD4 (RM4-5, Biolegend), Pacific Blue™ anti-CD8a (53-6.7, Biolegend), PE anti-CD45 (30-F11, Biolegend), Fluorescein labeled Peanut Agglutinin (PNA, VectorLaboratories), and Fixable Viability Dye eFluor® 780, APC conjugated anti-

CD19 (eBio1D3), FITC conjugated anti-CD38 (90), PE conjugated anti-CXCR4 (2B11), eFluor® 450 conjugated anti-CD45R/B220 (RA3-6B2), PE-Cy7 conjugated CD23 (B3B4), FITC conjugated anti-CD21/CD35 (eBio4E3), and PE conjugated anti-CD3e (145-2C11) all from ebio/Affymetrix. The following fluorescent-labeled anti-human antibodies were used: APC anti-CD45 (2D1), FITC anti-CD19 (HIB19), Pacific Blue™ anti-CD20 (HI47), PE anti-HLA-DR (LN3), and Hu FCR binding inhibitor purified all from ebio/Affymetrix. Data were acquired on CyAn ADP (Beckman Coulter) or LSR FORTESSA (BD) flow cytometers and analyzed with the FlowJo software package (TreeStar).

Treatment of mice with antibodies

Anti-mouse CD4 (BE0119, Clone: YTS) and rat IgG2b isotype control (BE0090, Clone: LTF-2) antibodies were purchased from BioXCell. Mice were administered a 500µg dose one day before i.v. injection of tumor cells, then once per week with a 250µg until end of the study (28 days), or starting only once palpable tumors had formed.

Ki67 staining of germinal centers

CONFIRM anti-Ki-67 (30-9) Rabbit Monoclonal Primary Antibody (Roche) was used for staining of proliferating cells within germinal centers on formalin-fixed paraffin-embedded spleen sections using a Ventana automated slide stainer. This was provided as a service by the Laboratory for Animal Model Pathology (LAMP) of the Institut für Veterinärpathologie of the University of Zürich. Three sections approximately 100 µm apart were assessed per mouse spleen. The images were acquired on a Leica microscope and Image J was used for area assessment. Germinal centers were identified as Ki67-positive areas within blue areas. Background staining, mostly on the peripheries of the spleen sections was not included.

ChIP-PCR

ChIP was performed as previously described (19). 100 x10^6 cells were fixed with 1% formaldehyde, lysed, and sonicated (Branson Sonicator; Branson), resulting in sheared chromatin of an average size of 200 bp. 2 µg of antibodies H3K27ac (ab4729, Abcam), and H3K18ac (ab1191, Abcam), or control rabbit IgG (sc-2027, Santa Cruz Biotechnology) were added to 25 µg of precleared sample and immunoprecipitated overnight at 4 °C. The complexes were purified using protein A beads (Invitrogen) followed by elution from the beads and decrosslinking. DNA was purified using PCR purification columns (Macherey Nagel) and quantified by quantitative PCR. The following primers were used for qPCR: GAPDH, fwd: AGA AGG CTG GGG CTC ATT TG, rev: AGG GGC CAT CCA CAG TCT TC; MyoD, fwd: CCT CTT TCG GTC CCT CTT TC, rev: TTCCAAACCTCTCCAACACC; XL4, fwd: CAG AGA AAG GGA ACT GAA AGT CAT TT, rev: TTA TGA CAC TGT TTA GTC CTA GAA CAC TGA; -600bp, fwd: ATG AGA TAC AAT GCC AGC CAT CC, rev: ACA GTT GGA GAG TTT GCG TAA GG; -300bp, fwd: TGT CCC TTA CGC AAA CTC TCC, rev: ACA CAA GAT ACT CCG TTC ATT GG; WXY, fwd: GAT CTC TTG TGT CCT GGA CCC TTT GCA AGA ACC CT, rev: CCC AAT TAC TCT TTG GCC AAT CAG AAA AAT ATT TTG; +1500bp, fwd: CTC CGT CTC AAA CAA CCA AAC C, rev: ACC AAC ACC AAG GGA ATA ATG AAC; +3500bp, fwd: TTC CGC AAG TTC CAC TAT CTC C, rev: CGA GTT TCA CAC AAG CAT CAT AGG.

Statistics

All statistical analyses were performed using Graph Pad Prism software. Graphs represent means plus SD of at least two independent experiments and statistical analysis was performed using two-tailed student's t-test for RT-PCR data, and using two-tailed Mann-Whitney test for *in vivo* studies. Cox regression analysis and the log-rank test were performed on patient cohorts to determine survival probability in multivariate and univariate analyses, respectively.

Data availability

The RNA-sequencing dataset is publicly available on the GEO Accession viewer with the accession number GSE89879.

(http://www.ncbi.nlm.nih.gov/geo/query/acc.cgi?acc=GSE89879).

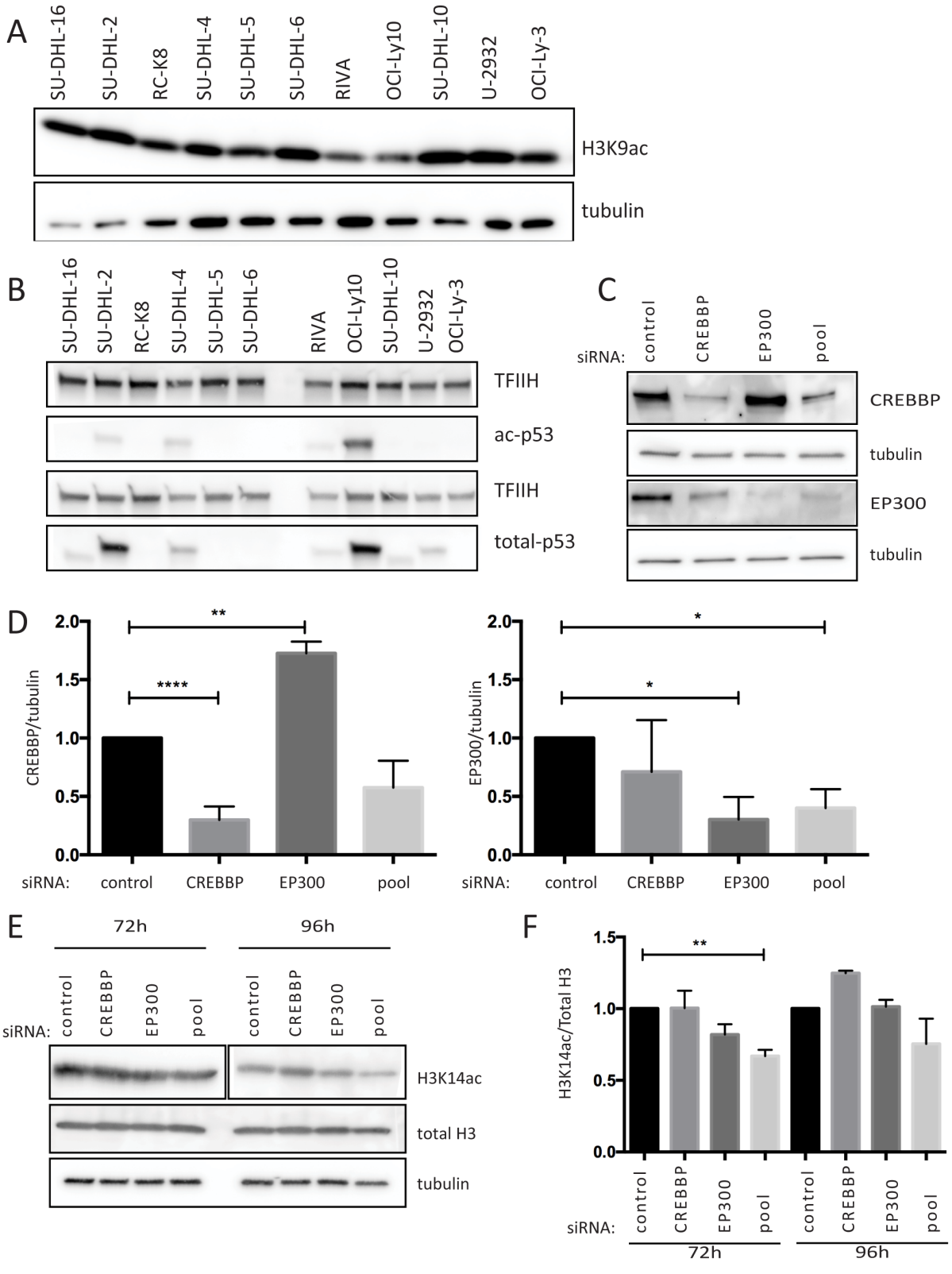
A
SU-DHL-16
SU-DHL-2
RC-K8
SU-DHL-4
SU-DHL-5
SU-DHL-6
RIVA
OCI-Ly10
SU-DHL-10
U-2932
OCI-Ly-3
H3K9ac
tubulin
B
TFIIH
ac-p53
TFIIH
total-p53
C
siRNA:
control
CREBBP
EP300
pool
CREBBP
tubulin
EP300
tubulin
D
CREBBP/tubulin
EP300/tubulin
**
****
*
*
2.0
1.5
1.0
0.5
0.0
E
72h
96h
H3K14ac
total H3
tubulin
F
H3K14ac/Total H3
**
1.5
1.0
0.5
0.0
72h
96h

Fig. S1.

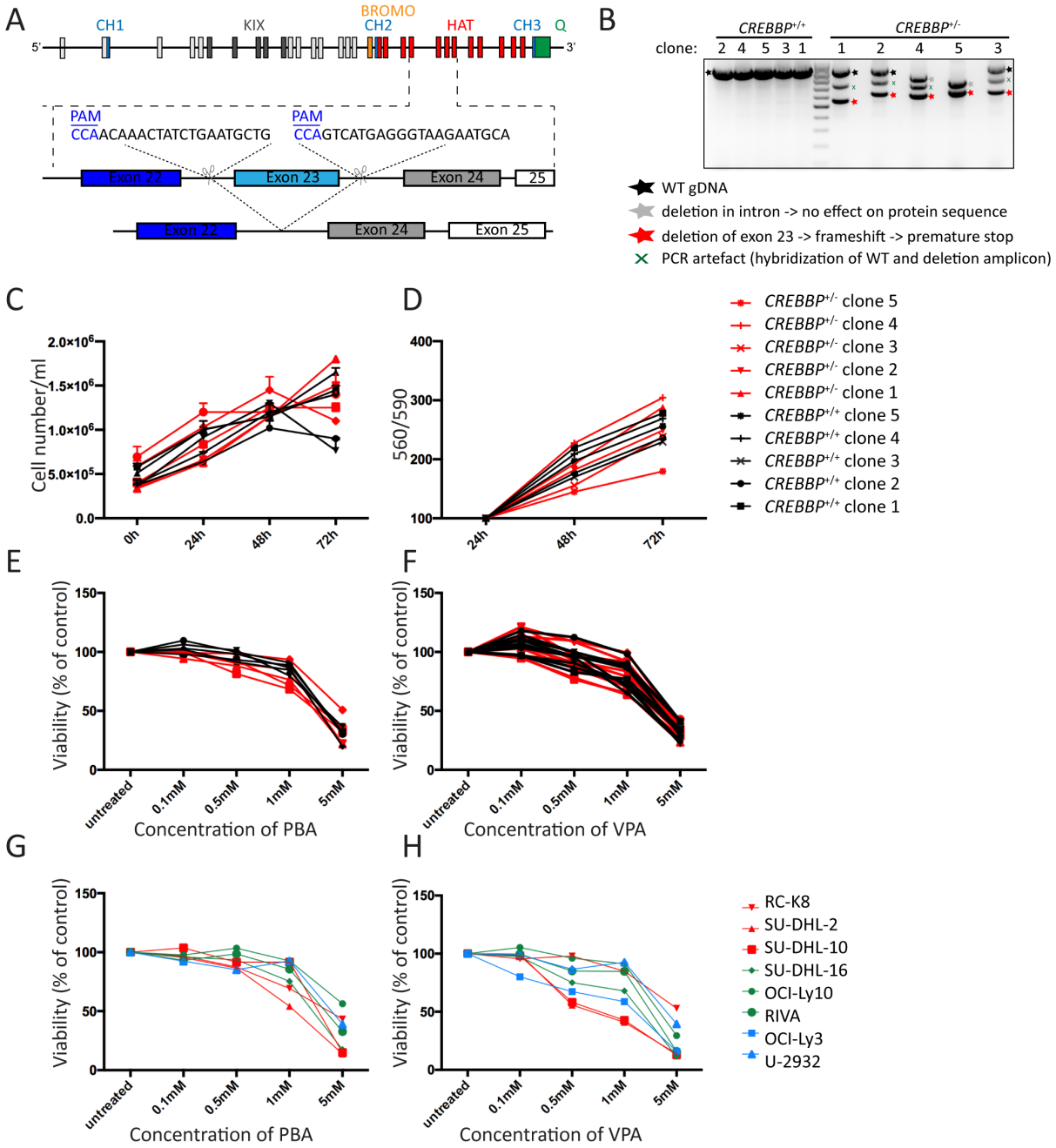
A
CH1
KIX
BROMO
CH2
HAT
CH3
Q
5'
3'
PAM
CCAACAAACTATCTGAATGCTG
PAM
CCAGTCATGAGGGTAAGAATGCA
Exon 22
Exon 23
Exon 24
25
Exon 22
Exon 24
Exon 25
B
clone:
CREBBP+/+
CREBBP+/-
2 4 5 3 1
1 2 4 5 3
WT gDNA
deletion in intron -> no effect on protein sequence
deletion of exon 23 -> frameshift -> premature stop
PCR artefact (hybridization of WT and deletion amplicon)
C
Cell number/ml
2.0×10^6
1.5×10^6
1.0×10^6
5.0×10^5
0.0
0h
24h
48h
72h
D
560/590
400
300
200
100
24h
48h
72h
CREBBP+/- clone 5
CREBBP+/- clone 4
CREBBP+/- clone 3
CREBBP+/- clone 2
CREBBP+/- clone 1
CREBBP+/+ clone 5
CREBBP+/+ clone 4
CREBBP+/+ clone 3
CREBBP+/+ clone 2
CREBBP+/+ clone 1
E
Viability (% of control)
150
100
50
0
untreated
0.1mM
0.5mM
1mM
5mM
Concentration of PBA
F
Viability (% of control)
150
100
50
0
untreated
0.1mM
0.5mM
1mM
5mM
Concentration of VPA
G
Viability (% of control)
150
100
50
0
untreated
0.1mM
0.5mM
1mM
5mM
Concentration of PBA
H
Viability (% of control)
150
100
50
0
untreated
0.1mM
0.5mM
1mM
5mM
Concentration of VPA
RC-K8
SU-DHL-2
SU-DHL-10
SU-DHL-16
OCI-Ly10
RIVA
OCI-Ly3
U-2932

Fig. S2.

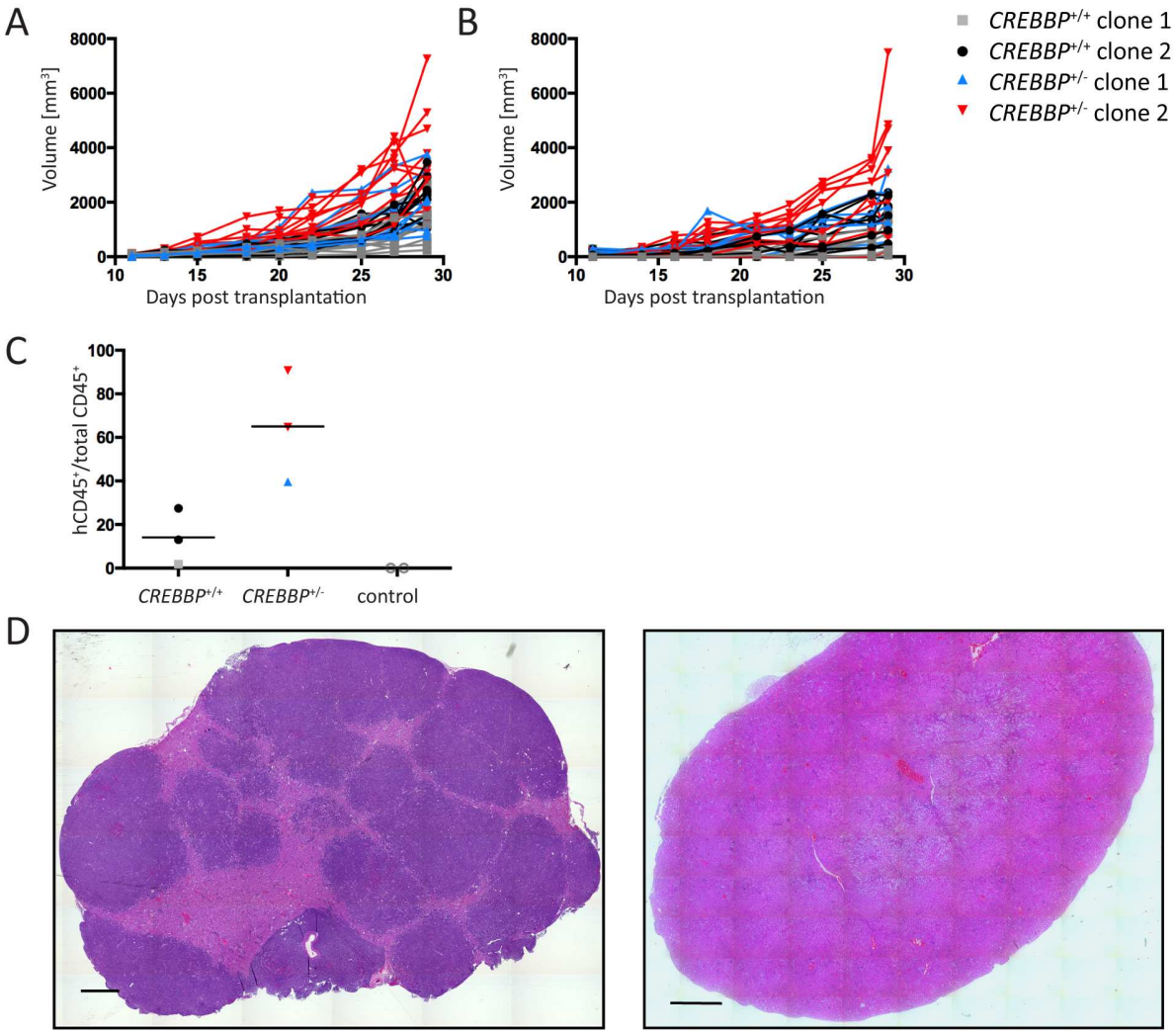
A
B
C
D
Volume [mm³]
Days post transplantation
CREBBP+/+ clone 1
CREBBP+/+ clone 2
CREBBP+/- clone 1
CREBBP+/- clone 2
hCD45+/total CD45+
CREBBP+/+
CREBBP+/-
control

Fig. S3.

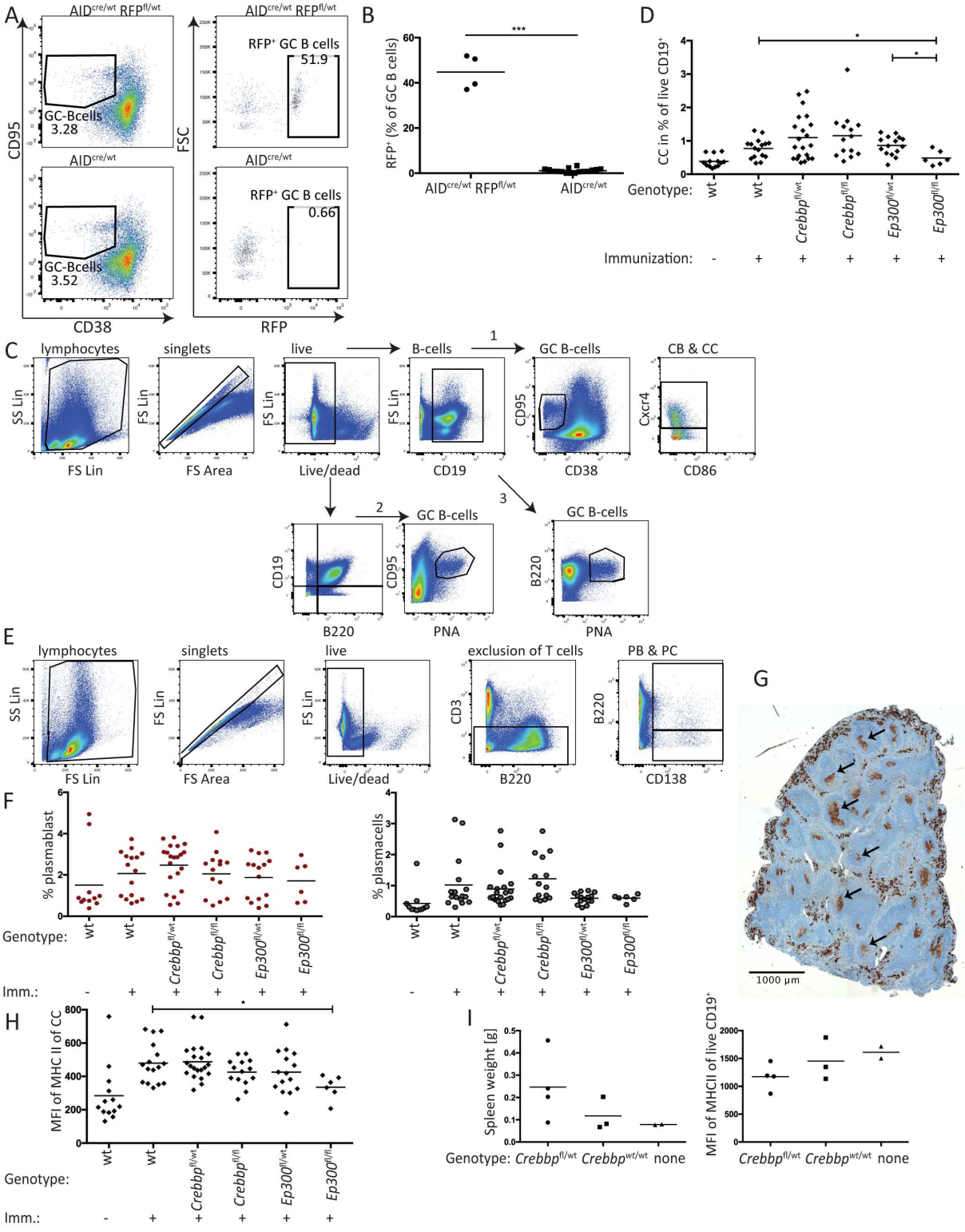
A
AIDcre/wt RFPfl/wt
GC-Bcells 3.28
GC-Bcells 3.52
CD95
CD38
FSC
RFP
RFP+ GC B cells 51.9
RFP+ GC B cells 0.66
B
RFP+ (% of GC B cells)
***
AIDcre/wt RFPfl/wt
AIDcre/wt
D
CC in % of live CD19+
Genotype:
wt
wt
Crebbpfl/wt
Crebbpfl/fl
Ep300fl/wt
Ep300fl/fl
Immunization:
C
lymphocytes
singlets
live
B-cells
GC B-cells
CB & CC
SS Lin
FS Lin
FS Area
Live/dead
CD19
CD95
CD38
Cxcr4
CD86
PNA
B220
E
exclusion of T cells
PB & PC
CD3
CD138
F
% plasmablast
% plasmacells
Imm.:
G
1000 µm
H
MFI of MHC II of CC
I
Spleen weight [g]
Genotype: Crebbpfl/wt Crebbpwt/wt none
MFI of MHCII of live CD19+

Fig. S4.

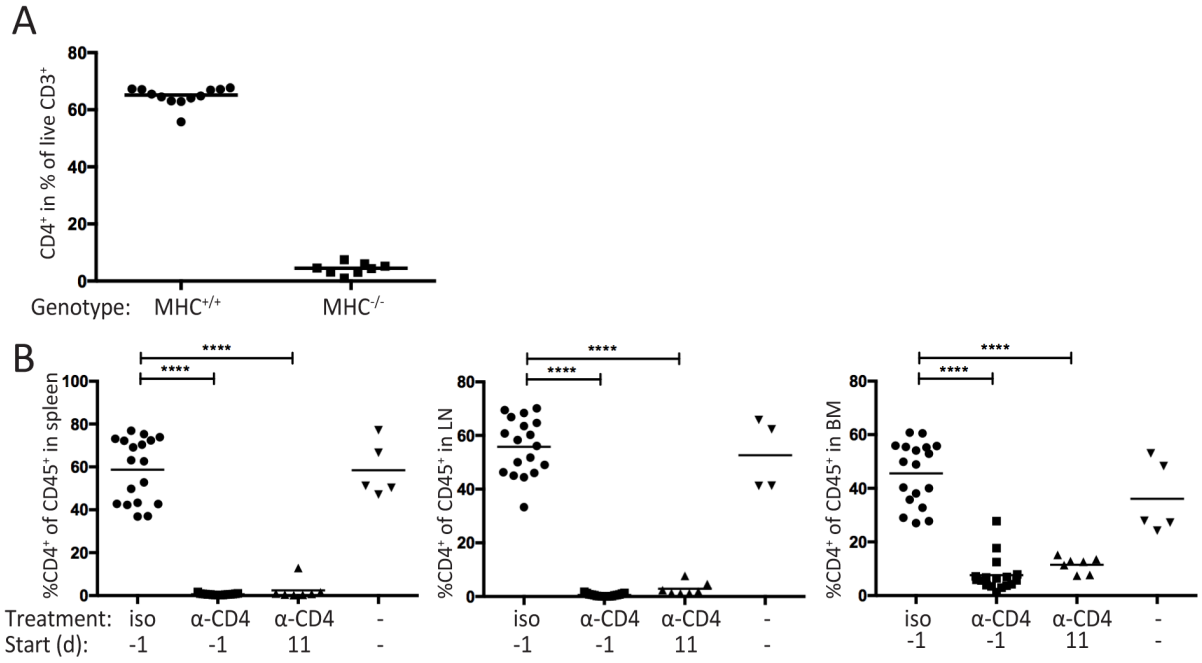
A
CD4+ in % of live CD3+
Genotype: MHC+/+ MHC-/-
B
%CD4+ of CD45+ in spleen
%CD4+ of CD45+ in LN
%CD4+ of CD45+ in BM
****
Treatment: iso α-CD4 α-CD4 -
Start (d): -1 -1 11 -

Fig. S5.